



ELSEVIER

Journal of Magnetism and Magnetic Materials 238 (2002) 293–300



www.elsevier.com/locate/jmmm

Effects of the progressive substitution of La^{3+} by Gd^{3+} in the magnetic and transport properties of $\text{La}_{2/3}\text{Ca}_{1/3}\text{MnO}_3$

L.E. Hueso^a, J. Rivas^{a,*}, P. Sande^a, A. Fondado^a, F. Rivadulla^b,
M.A. López-Quintela^b

^aDepartamento de Física Aplicada, Universidad de Santiago de Compostela, 15706 Santiago de Compostela, Spain

^bDepartamento de Química-Física, Universidad de Santiago de Compostela, 15706 Santiago de Compostela, Spain

Received 8 August 2001

Abstract

A systematic study of the magnetic and transport properties of the system $(\text{La}_{1-x}\text{Gd}_x)_{0.67}\text{Ca}_{0.33}\text{MnO}_3$ ($0 \leq x \leq 1$) is presented in this article. Through this series, a great crystallographic distortion is achieved but keeping constant the electronic density. At low Gd^{3+} content, these ions behaves in a paramagnetic state following a Brillouin function. Low-temperature ferromagnetism remains unchanged. However, for the samples with large Gd^{3+} content a complex magnetic behavior arises from several competing interaction as super-exchange, double-exchange and also the interaction between Gd and Mn ions. Resistivity and thermopower follow a progressive increase as Gd^{3+} content does, but the polaron energy in the paramagnetic range remains independent of all these changes. Thermopower infinite value is also determined and analyzed. © 2002 Elsevier Science B.V. All rights reserved.

Keywords: Magnetic properties; Transport properties; Substitution

1. Introduction

The experimental magnetic and transport properties of mixed-valence manganites have been studied in great detail in the last decade, and there have been many theoretical work in order to understand the intriguing properties they offer [1]. Most of this has been centered until now on the $\text{La}_{2/3}\text{Ca}_{1/3}\text{MnO}_3$ compound [2], as it presents a ferromagnetic–paramagnetic first-order transition related with high values of magnetoresistance, the

as-known colossal magnetoresistance (CMR) [3]. However, many other cations can be accommodated in the structure and the phase diagram of other compounds as $\text{La}_{1-x}\text{Sr}_x\text{MnO}_3$ [4], $\text{Pr}_{1-x}\text{Ca}_x\text{MnO}_3$ [5], etc., had been completed very quickly. In all these studies arises the deep relation between structure, magnetism and electronic transport. Following this trend of work, more specific studies came up with the purpose of studying one of the main contribution to the physical properties of manganites. This is the change in the crystallographic structure but maintaining a fixed doping level. Several authors completed a great number of different cationic substitutions [6–9], that can be briefly summarized

*Corresponding author. Tel.: +34-981-563100; fax: +34-981-520676.

E-mail address: farivas@usc.es (J. Rivas).

in the phase diagram proposed by Hwang et al. [6]. In all these works, the band filling is kept constant, but the electronic transfer, that is governed mainly by the mean Mn–O–Mn angle can be changed considerably by the different radii of the cationic substitutions [10]. All these experiments were completed by others where external pressure (rather than the internal chemical distortion) is varied [11,12]. All the conclusions mainly abounded in the interplay between structure and electronic transport.

In this work we decided to perform a systematic study of the structural, magnetic and electrical properties of $(\text{La}_{1-x}\text{Gd}_x)_{2/3}\text{Ca}_{1/3}\text{MnO}_3$ ($0 \leq x \leq 1$). By this way, the starting point of the serie is one of the prototypical CMR manganites with an optimal doping level. The progressive substitution of La^{3+} for Gd^{3+} is a particular favorable case, since the Gd^{3+} ion has $L = 0$, and therefore no complications are caused by the crystalline field. On the other hand, the Gd substitution in $\text{La}_{2/3}\text{Ca}_{1/3}\text{MnO}_3$ produces a continuous distortion in the structure due to its smaller ionic radio. The result are important changes both in the magnetic and transport properties of the original manganite. Moreover, the magnetic character of Gd^{3+} ions appears superimposed to the interactions between $\text{Mn}^{3+/4+}$ ions, generating new consequences.

2. Experimental

For this study we synthesize a serie of polycrystalline samples with nominal composition $(\text{La}_{1-x}\text{Gd}_x)_{0.67}\text{Ca}_{0.33}\text{MnO}_3$ ($x = 0, 0.10, 0.25, 0.50, 0.75, 1$). All of them were prepared by solid state reaction starting from high purity oxides and with a final sintering treatment at 1300°C for 100 h. X-ray Rietveld refinements show single phase materials in all the cases. Magnetic measurements were done in a SQUID magnetometer. Resistivity was measured by the standard four-probe method with gold contacts. Measurements of thermoelectric power were performed with a home-made apparatus and a temperature difference of 1 K was applied between two parallel cuts of each sample.

3. Results and discussion

3.1. Structural properties

The substitution of La^{3+} ions by Gd^{3+} leads to a progressive reduction of the tolerance factor, t , as a consequence of the decrease of the mean ionic radio $\langle r_A \rangle$. This distortion in the perovskite structure corresponds to a decrease in the mean Mn–O–Mn bonding angle (see Table 1). As the electronic doping level remains unchanged, and so the band filling, the structural distortion is the main responsible of the changes in the magnetism and in the transport properties, as we shall discuss after. All the following results have to be linked with this previous one.

3.2. Magnetic properties

Firstly, we are going to revise the basic magnetic properties in the whole serie of samples. The temperature dependence from 5 up to 350 K of the magnetization is measured after cooling in zero magnetic field (ZFC) and after cooling in a field (FC) are reported in Fig. 1. It seems clear from the data exposed that samples can be divided into two different groups: the ones with small Gd percentage (0%, 10% and 25%) and the others with high Gd content (i.e. 50%, 75% and 100%). The first group includes samples that shows a clear transition from a high-temperature paramagnetic state down to a ferromagnetic one. Although the Curie temperature is shifted down as Gd increases, the

Table 1

Mean ionic radii, tolerance factor and mean Mn–O–Mn angle for several Gd content. It is clear that there is continuous reduction in all the structural parameters as Gd content increases

Gd percentage (%)	$\langle r_A \rangle$	t	Mean Mn–O–Mn angle (deg)
0	1.204	0.917	159.7
10	1.197	0.915	158.6
25	1.186	0.911	157.3
50	1.167	0.901	155.5
75	1.149	0.897	152.7
100	1.131	0.896	150.9

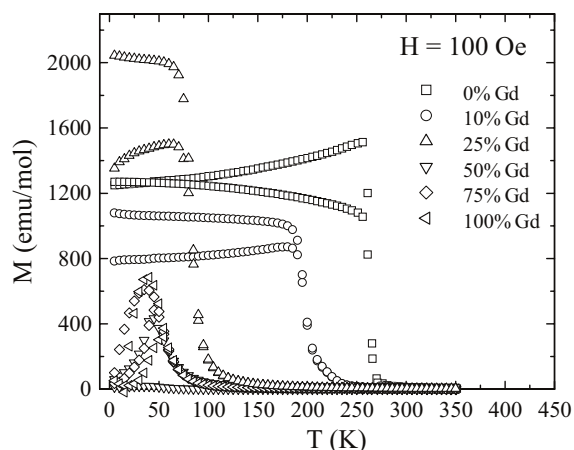


Fig. 1. Zero-field-cooled-field-cooled (ZFC-FC) measurements for the samples with different Gd percentage.

samples present a long-range ferromagnetic state at low temperature with none indication of inhomogeneous magnetic state. In contrast, the samples of the second group present a maximum in both ZFC and FC curves around 50 K (see Fig. 2). All these results seems to fit perfectly with the phase diagram proposed by Hwang et al. and with similar results from other authors [6,13]. The main point in this case is the decrease in both FC and ZFC curves below transition temperature, where magnetization presents a peak. The increasing crystallographic distortion favor the interaction between the Mn and Gd ions and could bring about the Mn to undergo a spontaneous spin reorientation that is reflected in the FC-ZFC peak, as has been seen in other compounds like Gd_2CuO_4 [14,15], or orthoferrites [16]. This effect is only present when the structure is very distorted and the antiferromagnetic superexchange (SE) contribution between Mn ions is much larger than the ferromagnetic double-exchange (DE) one. From low-temperature hysteresis loops in fields up to 50 kOe (Fig. 3) we can separate the same two groups of samples. The group one, that is, the samples with low Gd content, show the typical ferromagnetic curve, although a paramagnetic component is observable. This contribution arises from the Gd ions, that behave as purely paramagnetic in the low doping range. But again, the

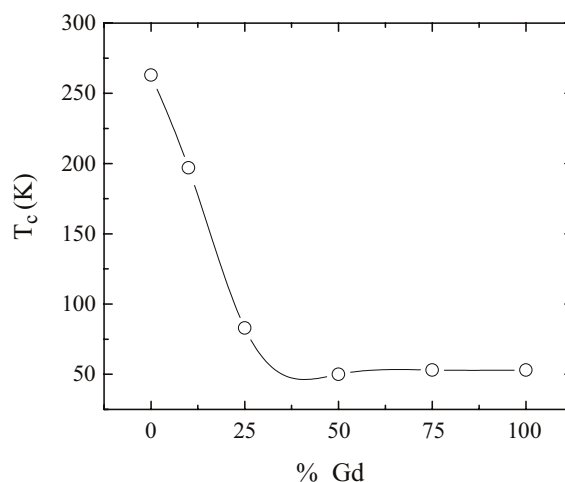


Fig. 2. Critical transition temperature versus gadolinium percentage.

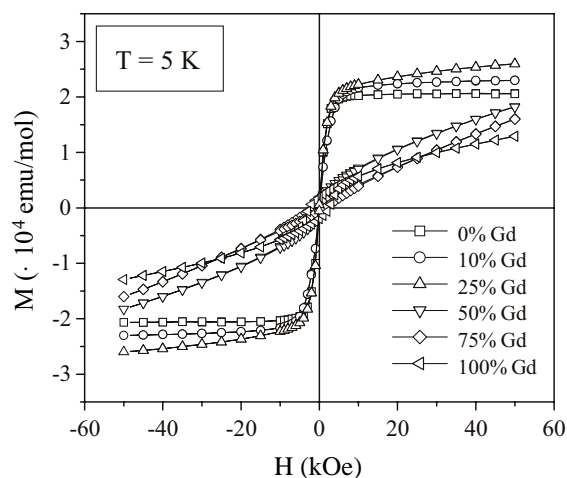


Fig. 3. Magnetization hysteresis loops at $T = 5$ K for all the samples studied.

samples with larger Gd percentage present a complex magnetic behavior. We believe this is the result of the competing magnetic interactions in that scenario, the ferromagnetic DE, the antiferromagnetic SE and also, the interaction between Gd^{3+} spins and the ordered $\text{Mn}^{3+/4+}$ ions. First of all, we have carefully studied the magnetic response of low doped samples in order to understand the possible paramagnetism of

Gd³⁺ ions. Demagnetizing factor (*D*) was estimated in terms of a phenomenological approach [17], and values for *D* between 3.1 and 4.3 were taken in account in order to correct magnetization hysteresis loops. In large fields, the reference measurement in the sample without any Gd content was fitted to saturation approach law [18],

$$M = M_s \left(1 - \frac{a}{H} - \frac{b}{H^2} \right), \tag{1}$$

where *a* and *b* are suitable constants. In the specific case of the experimental magnetization at *T* = 5 K of the reference compound La_{2/3}Ca_{1/3}MnO₃, fits gave a result of *a* = 142 ± 8 Oe, *b* = 20 510 ± 500 Oe² and *M_s* = 20 660 ± 30 emu/mol. Samples with 10% and 25% of Gd content can be fitted assuming two different parts, so their total magnetization should be the sum of the Mn^{3+/4+} contribution (*M_{Mn}*) plus the Gd³⁺ one (*M_{Gd}*), as

$$M = M_{Mn} + M_{Gd}. \tag{2}$$

With this protocol it is possible to separate the contribution of Gd ions, subtracting from the total magnetization the data corresponding to % Gd = 0, and to study them alone. If Gd³⁺ ions are well magnetically diluted in a paramagnetic state rather than correlated to Mn lattice for this concentrations, they will have to obey the well-known saturation law of paramagnetic substances [18],

$$M_{Gd} = Ng\mu_B J \left[\frac{2J+1}{2J} \coth \left(\frac{2J+1}{2J} y \right) - \frac{1}{2J} \coth \left(\frac{1}{2J} y \right) \right], \tag{3}$$

where *N* is the number of paramagnetic ions, *g* is the gyromagnetic ratio for the electron (≈ 2), μ_B is the Bohr magneton, and *J* is the atomic angular momentum quantum number (in this specific case, the Gd³⁺ has *L* = 0 and therefore *J* = *S* = 7/2). Moreover,

$$y = \frac{Jg\mu_B H}{k_B T}, \tag{4}$$

where *k_B* is the Boltzman constant. With this expression (3) of the Brillouin function, we can obtain information about the magnetic properties of Gd³⁺ ions (Fig. 4). For example, in Fig. 5,

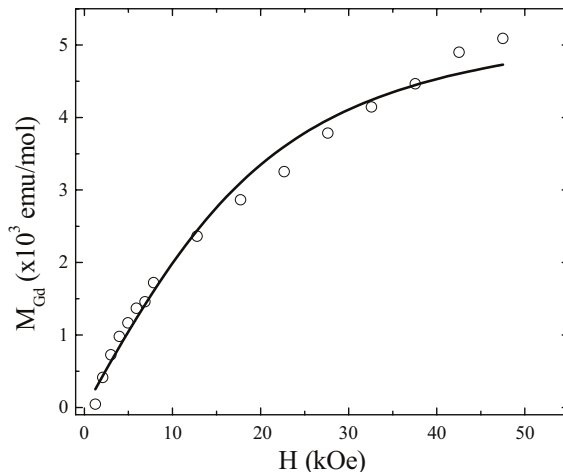


Fig. 4. Magnetization of Gd³⁺ ions (open circles) obtained after subtracting the contribution of Mn^{3+/4+} ions from the total magnetization as mentioned in the text (Eq. (2)) for the sample with Gd = 25%. The solid line indicates the best fit to Brillouin function.

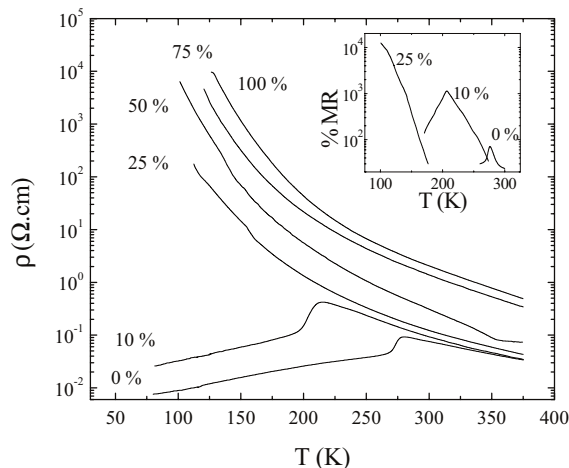


Fig. 5. Thermal dependence of resistivity for all the samples. (Inset) Magnetoresistance (*H* = 10 kOe) versus temperature curves for the samples with less Gd content.

presents the magnetization of Gd³⁺ ions in the sample of 25% after subtracting the contribution of Mn ions from the total magnetization. In the same graph appears the fit to the already cited Brillouin function. The results obtained of the only free parameter in Eq. (3) (*N*, number of paramagnetic ions) can be compared with the theoret-

tical one calculated from the stoichiometry of the samples. The experimental data for the samples with 10% and 25% of Gadolinium are $(4.5 \pm 0.4) \times 10^{22}$ and $(8.2 \pm 0.3) \times 10^{22} \text{ mol}^{-1}$, respectively, and the predicted are 3.0×10^{22} and $7.4 \times 10^{22} \text{ mol}^{-1}$ for the same ones. As it was observed, the data do not match perfectly, but they show the clear tendency described above. The important result is that Gd^{3+} ions are behaving without interactions between them at low concentrations levels and so, their behavior is reproducible in their main aspects with pure paramagnetic laws.

3.3. Transport properties

First of all, we have to analyze the electrical resistivity data of the whole serie of samples prepared. In Fig. 5, we show resistivity data from 375 down to 77 K. Temperature where metal–insulator transition takes place (T_{M-I}) is reduced when Gd doping is increased, and for values up to 10% it totally disappears from our experimental data range. Resistivity values also increase manifestly with Gd doping. As we indicate before, these are well-known results in $\text{La}_{2/3}\text{Ca}_{1/3}\text{MnO}_3$ substituted manganites with Gd or other smaller size ions [6–9]. Correspondingly, the magneto-resistance effect, is defined as $\%MR = ((R(H=10 \text{ kOe}) - R(H=0))/R(H=10 \text{ kOe}))$, is also increased as T_{M-I} is reduced (see Fig. 5, inset). This is also an expected result that tests the relation between structure and the lattice effects that governs the CMR effect [6–8,19]. In the paramagnetic range, Emin and Holstein calculated resistivity in the adiabatic regime and found a mobility with thermally activated form [20], that directs to

$$\rho(T) = \rho_0 T \exp(E_\rho/kT), \quad (5)$$

where E_ρ is the activation energy, and the resistivity prefactor ρ_0 depends on the concentration of polarons, the hopping distance and the frequency of the longitudinal optical phonons. Resistivity in the semiconductor range was satisfactorily fitted by small-polaron hopping equation (Eq. (5)) and the activation energy value are shown

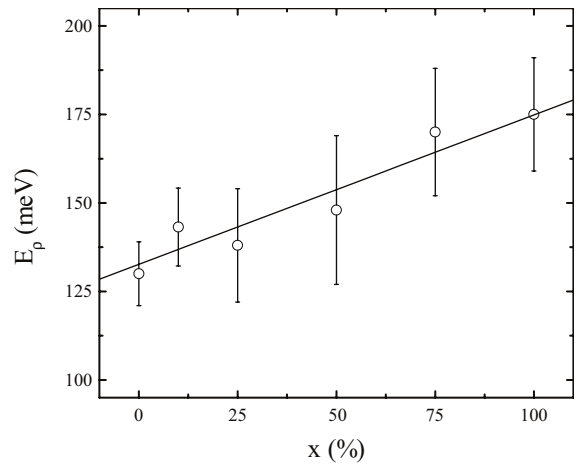


Fig. 6. Variation of resistivity activation energy with Gd percentage. Line is a linear fit to the data.

in Fig. 6. Activation energy for resistivity increase as Gd percentage does.

The second transport property studied is thermopower. In a case of thermally activated conduction, it takes the form:

$$S = \frac{k}{e} \left(\frac{E_S}{kT} \right) + S_\infty, \quad (6)$$

where E_S is again the activation energy (that differ from resistivity one, not as in the case of classical semiconductors) and S_∞ is the thermopower high-temperature limiting value [21,22]. From a careful study of both resistivity and thermopower measurements it is possible to understand the polaronic nature of conductivity in manganites and to enlighten some of the points that remains without a clear explanation.

In Fig. 7, we plot the thermopower temperature dependence. Low doping rate samples present a transition almost coincident with T_C and T_{M-I} (see inset). However, it is noticed that the change in the sign observed around that temperature is not related with a change in the carriers nature but on the competition between the entropic term and the energy transport term of the thermopower [22]. The values in the metallic range are constant and small, around a few $\mu\text{V/K}$, as is typical in these systems.

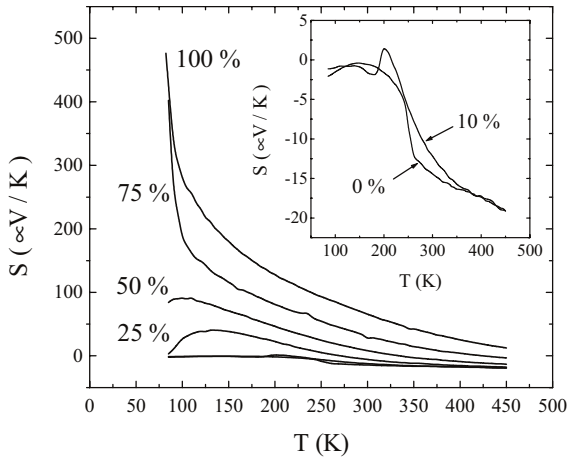


Fig. 7. Thermal dependence of thermopower for all the samples studied. (Inset) Thermopower versus temperature curves for the samples with less Gd content.

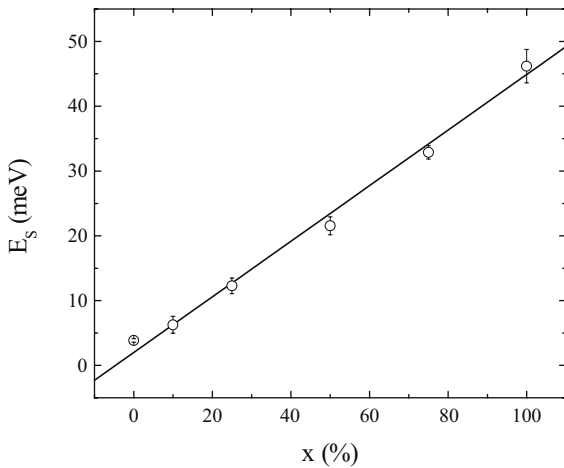


Fig. 8. Variation of thermopower activation energy with Gd percentage. Line is a linear fit to the data.

If we study the paramagnetic span, the values are very high and coincident with the reduced carrier mobility viewed through resistivity [23]. All the samples can be accurately fitted to Eq. (6). Activation energy values for the thermopower are depicted in Fig. 8, and the high-temperature limiting value S_∞ is also shown in Fig. 9. With these results, we have to focus in the possible explanations and the consequences derived from them. From the fits employing Eq. (6), it is unambiguous

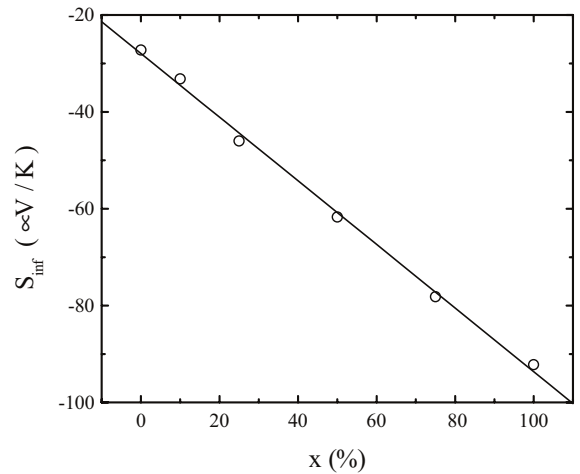


Fig. 9. Thermopower infinite temperature limiting value versus Gd content. Line is a linear fit to the data.

again that the linear dependence is obtained between the doping level and S_∞ . However, this result has to be studied very carefully, as other measurements up to 1000 K realized by other groups suggest a common infinite temperature value for samples with different tolerance factor [24,25].

The values obtained are always negative and should reflect the combination of several contributions, generally [26,27]:

$$S_\infty = S_\sigma + S_{ME}. \tag{7}$$

The first term (S_σ) is determined by the configurational entropy of placing a spin σ_1 hole in a spin σ_0 background, and it is given by

$$S_\sigma = \left(\frac{k}{e}\right) \ln\left(\frac{2\sigma_1 + 1}{2\sigma_0 + 1}\right) \tag{8}$$

in our specific case, the right values are $\sigma_1 = 3/2$ and $\sigma_0 = 2$, leading to a final value of $S_\sigma = -19.2 \mu\text{V/K}$. The second term (S_{ME}) is the mixing entropy term that counts in how many different ways x holes can be distributed between n sites. There are several alternative models considered in the bibliography, like the Heikes correlated limit [27,28], the Heikes uncorrelated limit [22,27–29], that has been usually employed by several groups, and the Chaikin–Beni expression

[21,29]. This is probably the most accurate theoretical approach to this problem, as it considers fermions with spin, but with on-site repulsion, so that two electrons with either spin parallel or opposed are forbidden double occupancy of a single site. The results proposed is given by

$$S_{\text{ME}} = \left(\frac{k}{e}\right) \ln\left(\frac{2(1-x)}{x}\right). \quad (9)$$

For our constant doping ($x = 0.33$), this mixing entropy term contributes $S_{\text{ME}} = -120.0 \mu\text{V/K}$ to the total thermopower infinite-temperature limit. So, the total result will be $S_{\infty} \approx -140 \mu\text{V/K}$. As it is denoted, this result reflects the sign of the thermopower, but not none of the absolute values obtained from our fits, or even the temperature-independent values suggested in other publications [24,25].

At a fixed doping value, all the models cited before supports a constant value, so they cannot predict the linear fit obtained from our experimental data. However, we could try to understand this behavior not forgetting the crystallographic distortion induced by Gd doping, that is not taken into account in the development of the theoretical expressions. The greater the distortion, the less accessible the hopping sites for the electrons, and so, the more important the entropy term that inform us about the disorder of the system, as it is suggested in our experimental result. In any case, new measurements at higher temperatures should have to be done in order to avoid uncertainties.

From the activation energies of resistivity and thermopower it is possible to obtain one of the fundamental parameter from the transport properties, that is, the small polaron formation energy in the paramagnetic range. In general, we can employ the relation [21]:

$$E_{\rho} = E_{\text{S}} + W_{\text{H}} - J, \quad (10)$$

where W_{H} is one-half of the polaron formation energy and J is the transfer integral. If we assume J to be much smaller than W_{H} , we conclude:

$$W_{\text{P}}/2 = W_{\text{H}} = E_{\rho} - E_{\text{S}}. \quad (11)$$

By this way, we have computed the polaron formation energy for all the samples studied (see

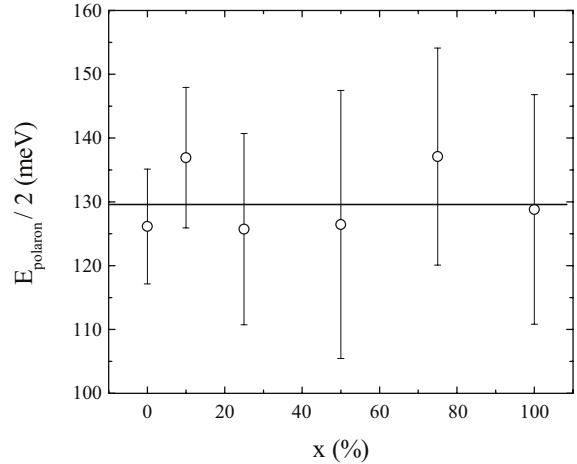


Fig. 10. Polaron hopping energy or half of the polaron formation energy. Line is again a linear fit.

Fig. 10). As is clearly seen, the obtained result is almost independent of the doping level, or in other way, of the distortion of the structure. Despite the great changes induced in the exchange interaction, that transform enormously the magnetism and the transport properties, this parameter seems to behave limitless from this dependence. This an exciting result that has to be interpreted theoretically in a proper way.

4. Conclusions

Systematic study of the structural, magnetic and transport properties on the system $(\text{La}_{1-x}\text{Gd}_x)_{0.67}\text{Ca}_{0.33}\text{MnO}_3$ ($0 \leq x \leq 1$) were reported. These measurements indicate the progressive distortion of the perovskite structure as Gd^{3+} content increases and a clear change in the magnetism and transport linked with this effect. Magnetic properties allows us to define two sets of samples, the group with Gd content up to 25% and the ones. The first ones present a ferromagnetic low-temperature state derived from the double-exchange interaction between $\text{Mn}^{3+}/\text{Mn}^{4+}$ ions, plus a paramagnetic contribution arising from the Gd^{3+} ions. The second group reveals complex magnetic behavior resulting from the dominant antiferromagnetic

superexchange plus the reminiscent double exchange and the interaction involving the Gd and the Mn ions together. The transport properties studied (resistivity and thermopower) reveals a gradual destruction of electronic conductivity mainly due to the already cited crystallographic distortion. Both activation energies increase with Gd^{3+} percentage, but the already calculated polaron energy in the paramagnetic range remains almost unchanged even when magnetic and transport properties are greatly modified. Finally, a tentative study of high-temperature limiting thermopower values is presented.

References

- [1] J.M.D. Coey, M. Viret, S. von Molnar, *Adv. Phys.* 48 (1999) 167.
- [2] P. Schiffer, A.P. Ramirez, W. Bao, S.-W. Cheong, *Phys. Rev. Lett.* 75 (1995) 3336.
- [3] S. Jin, T.H. Tiefel, M. McCormack, R.A. Fastnacht, R. Ramesh, J.H. Chen, *Science* 264 (1994) 413.
- [4] A. Urushibara, Y. Moritomo, T. Arima, A. Asamitsu, G. Kido, Y. Tokura, *Phys. Rev. B* 51 (1995) 14103.
- [5] Y. Tomioka, A. Asamitsu, H. Kuwahara, Y. Moritomo, Y. Tokura, *Phys. Rev. B* 53 (1996) 1689.
- [6] H.Y. Hwang, S.-W. Cheong, P.G. Radaelli, M. Marezio, B. Batlogg, *Phys. Rev. Lett.* 75 (1995) 914.
- [7] J. Fontcuberta, B. Martinez, A. Seffar, P. Piñol, J.L. García-Muñoz, X. Obradors, *Phys. Rev. Lett.* 76 (1996) 1122.
- [8] J. Blasco, J. García, J.M. de Teresa, M.R. Ibarra, P.A. Algarabel, C. Marquina, *J. Phys.: Condens. Matter* 8 (1996) 7427.
- [9] J.R. Sun, J.H. Rao, J.K. Llang, W.Y. Zhou, *Appl. Phys. Lett.* 69 (1996) 3926.
- [10] P.W. Anderson, H. Hasegawa, *Phys. Rev.* 100 (1955) 675.
- [11] Y. Moritomo, A. Asamitsu, Y. Tokura, *Phys. Rev. B* 51 (1995) 16491.
- [12] J.S. Zhou, W. Archibald, J.B. Goodenough, *Nature* 381 (1996) 770.
- [13] M. Rubinstein, D.J. Gillespie, J.E. Snyder, T.M. Tritt, *Phys. Rev. B* 56 (1997) 5412.
- [14] J.D. Thomson, S.-W. Cheong, S.E. Brown, Z. Fisk, S.B. Oseroff, M. Tovar, D.C. Vier, S. Schultz, *Phys. Rev. B* 39 (1989) 6660.
- [15] S.B. Oseroff, D. Rao, F. Wright, D.C. Vier, S. Schultz, J.D. Thomson, Z. Fisk, S.-W. Cheong, M.F. Hundley, M. Tovar, *Phys. Rev. B* 41 (1990) 1934.
- [16] A.H. Cooke, D.M. Martin, M.R. Wells, *J. Phys. C* 7 (1974) 3133.
- [17] R.M. Bozorth, *Ferromagnetism*, IEEE Press, New York, 1993.
- [18] A.H. Morrish, *The Physical Principles of Magnetism*, New York, Wiley, 1965.
- [19] K. Khazeni, Y.X. Jia, L. Lu, V.H. Crespi, M.L. Cohen, A. Zettl, *Phys. Rev. Lett.* 76 (1996) 295.
- [20] D. Emin, T. Holstein, *Ann. Phys.* 53 (1969) 439.
- [21] M. Jaime, M.B. Salamon, M. Rubinstein, R.E. Treece, J.S. Horwitz, D.B. Chrisey, *Phys. Rev. Lett.* 54 (1996) 11914.
- [22] T.T.M. Palstra, A.P. Ramirez, S.-W. Cheong, B.R. Zegarski, P. Schiffer, J. Zaanen, *Phys. Rev. B* 56 (1997) 5104.
- [23] J. Fontcuberta, A. Seffar, X. Granados, J.L. García-Muñoz, X. Obradors, S. Piñol, *Appl. Phys. Lett.* 68 (1995) 2288.
- [24] W. Archibald, J.S. Zhou, J.B. Goodenough, *Phys. Rev. B* 53 (1996) 14445.
- [25] J.B. Goodenough, *Aust. J. Phys.* 52 (1999) 155.
- [26] M.F. Hundley, J.J. Neumeier, *Phys. Rev. B* 55 (1997) 11511.
- [27] M. Jaime, M.B. Salamon, *Physics of Manganites*, Kluwer, Academic/Plenum Publishers, New York, 1999.
- [28] R.R. Heikes, *Thermoelectricity*, Wiley, New York, 1965.
- [29] P.M. Chaikin, G. Beni, *Phys. Rev. B* 13 (1976) 647.